Journal of Metals, Materials and Minerals, 36(2), e2557, 2026

Sodium alginate/aloe vera/mangosteen peel extraction hydrogel composite films with anti-staphylococcal properties as a promising alternative material in biomedical applications

Pruss CHIMWAI[1], Poonyarat APIKARNSAKULCHAI[1], Tirawit JINDARATANAPORN[1], Witsanu LIANGAUMNUAY[1], Thitima LA-ONGTHITIRAT[1], Purin SOMNUAKE[2], and Pattara SOMNUAKE[3,*]

[1] *The Demonstration School of Bansomdejchaopraya Rajabhat University, Bangkok, 10600, Thailand.*
[2] *Department of Clinical Chemistry, Faculty of Medical Technology, Mahidol University, Phutthamonthon, Nakhon Pathom, 73170, Thailand*
[3] *School of Integrated Science and Innovation, Sirindhorn International Institute of Technology (SIIT), Thammasat University, Pathum Thani, 12120, Thailand*

***Corresponding author e-mail**: Pattara.somn@dome.tu.ac.th

Received date:
5 November 2025
Revised date:
25 December 2025
Accepted date:
13 February 2026

Keywords:
Hydrogel;
Sodium alginate;
Mangosteen peels;
Antibacterial;
Biomedical applications

Abstract

This study focuses on the development of alternative biodegradable hydrogel films from sodium alginate as a matrix and curing into a hydrogel by $CaCl_2$. Thus, the aloe vera (AV) and the crude extract of mangosteen peels (MPE) were additionally blended. The polymer films were prepared using the casting film process, and their morphology, functional groups, water absorption, antibacterial, thermal, and mechanical properties were characterized using SEM, FTIR, water swelling test, disk diffusion method, DSC-TGA, and UTM. The results demonstrated the heterogeneity between the composites and the polymer matrix, and a lower polarity from the decreased %water swelling from 45% to 22%. The mechanical properties showed that the rigidity and strength of the composites were improved, while those without particle blends showed a superior elongation at break. The DSC-TGA revealed a lower melting temperature, but a higher thermal degradation temperature when the additives were added to the films. The *Staphylococcus aureus* protection provided a clear inhibition zone of 15 ± 1 mm. Lastly, the results of polymer composites hydrogel demonstrated a potential for biomedical applications, particularly as wound dressing materials.

1. Introduction

Plastic waste has become a critical global environmental issue, and more than 430 million tonnes are produced annually. Plastic waste produces microplastics that affect the environment, including humans, marine animals, and plants [1,2]. Actually, biodegradable plastics are promising materials that can solve this problem. Almost all biodegradable plastics can be synthesized from natural sources such as corn, cassava, starch, and algae. Alginate is an anionic polysaccharide primarily extracted from brown seaweed, mainly harvested from species like Macrocystis pyrifera, Ascophyllum nodosum, and Laminaria varieties. It is arranged in blocks composed of two monomers of mannuronic acid (M) and guluronic acid (G), which form a linear chain. In specific details, chemically, sodium alginate (SA) is the sodium salt of alginic acid, composed of linear chains of β-D-mannuronic acid and α-L-guluronic acid units [3,4]. On the other hand, it was used to control the drug releasing in its delivery system and applied in the biomedical applications, such as wound dressings and tissue engineering scaffolds [5]. Because of its excellent biocompatibility, biodegradability, and non-toxic characteristics, it is particularly valuable for applications involving human contact.

Therefore, SA is an essential biomaterial due to the growing demand for natural, sustainable alternatives. Roopa, B. S., and Suvendu Bhattacharya casted a hydrogel film with 1% to 3% w/v of SA at 40°C, and water was then evaporated to let the SA form a thin film with a chain arrangement [6]. Wang, Hong, Liang Yang, and Yanning Yang described the crosslinking of the SA film by soaking it in a $CaCl_2$ solution at 1% to 2% w/v for 10-30 min. The SA crosslink arises from the ionic interactions between the polymer chains and multivalent cations of calcium ions (Ca^{2+}) [7]. The word "SA hydrogel" was used to definite the cross-linked SA film, which exhibited new characteristics of a high mechanical flexibility and water absorption without dissolving. Meanwhile, it was still biodegradable and environmental friendly [7,8]. However, SA hydrogel has some disadvantages, such as low mechanical properties and an inability to be antibacterial.

To overcome the limitations of neat SA, the incorporation of plant-based additives, such as aloe vera and mangosteen peel extracts has been investigated. The extensive use of plants has emerged as a topic of interest in modern biomedical materials as an approach to solving those disadvantages. The Aloe barbadensis Miller (Aloe vera, AV) contains 75 bioactive compounds, such as acemannan, a β-(1,4)-linked acetylated mannan that demonstrated significant immunomodulatory, anti-inflammatory, and wound-healing activities [9]. In addition, other beneficial compounds, including salicylic acid, amino acids, vitamins, and minerals, are present. Moreover, AV works synergistically with alginate's calcium-cross-linked network, rendering the material mechanically strong and biologically active. Other studies have reported that the blending of AV in the SA matrix increased mechanical strength when 20% aloe vera was added, and also improved the moisture barrier [10]. In terms of wound healing and antibacterial, Chelu, Mariana, *et al.*

demonstrated that the improved bioactivity and antibacterial properties of the material contributed to enhanced wound healing effects [11].

Some of the extracted compounds display the advantages of anti-oxidant and antimicrobial properties. It is an alternative natural material with potential applications in cosmetic skincare and biomedical fields [12-14]. Nguyen, Ha Thu, *et al.* consistently demonstrated that the incorporation of mangosteen rind extract into a cellulose hydrogel enhanced the thermal stability and provided effective antibacterial activity against both Gram-positive and Gram-negative bacteria [15]. Mangosteen peel, a byproduct of agricultural waste, accounts for approximately 60% to 70% of the total fruit weight. It represents an interesting source for the extraction of high-value bioactive compounds, including xanthones, tannins, anthocyanins, and phenolic acids [16-18]. Solvent extraction using alcohol was employed to extract the bioactive compounds due to its simplicity and high efficiency in producing the crude mangosteen peel extract (MPE). Other specific techniques, such as ultrasound-assisted extraction, supercritical CO_2, and microwave-assisted extraction, have increased yield and shortened extraction time. However, these methods require specialized equipment, making them challenging to apply on an industrial scale.

This study proposes the development of sodium alginate as a matrix material and cross-links it with $CaCl_2$ to fabricate hydrogel films. In addition, aloe vera and mangosteen peel extract were incorporated. The functional groups, chemical structures, water swelling, mechanical, thermal, and antibacterial properties against Staphylococcus aureus were investigated in the ternary hydrogel system with enhanced synergistic effects, which for a further alternative biodegradable wound dressing and biomedical materials.

2. Experimental

2.1 Materials

Sodium alginate (SA) particles (food-grade, non-GMO) were purchased from Chemrich, Thailand. Organic aloe vera extraction was supplied by Phitsanuchemicals Co., Ltd., Thailand. Mangosteen peels were obtained from the local market in Bangkok, Thailand. Calcium chloride ($CaCl_2$) was purchased from Suksapanpanit Co., Ltd., Thailand, while citric acid and ethanol (95%, technical grade) were obtained from Gammaco, Thailand. Ascorbic acid was supplied by Carlo Erba, Italy.

2.2 Extraction of MPE

Fresh mangosteen peels were dried in an oven at 80°C overnight, then milled to obtain dried peel powder. The MPE was prepared using 95% ethanol with an extraction method at 25% w/v. The mixture was stirred continuously at room temperature for 8 h, then filtered to separate the residue. The liquid phase was evaporated subsequently to remove the solvent at 80°C for 4 h. The crude MPE was obtained with about 10% to 12%yield from the dried mangosteen peels, which were used for further experiments.

2.3 Hydrogel films casting process

The SA solution was prepared by dissolving SA powder in distilled water 10% w/v at 45°C until it was clear, then cooling it to room temperature. For the AV blend films, AV extracted solution (pre-treated with 0.45% citric acid and 0.2% v/v ascorbic acid) was incorporated at 20% v/v of the alginate solution, along with 1 wt% MPE (ground and sieved with 50 μm nylon mesh before using). Then, the film solution was cast in a petri dish, as molds, and dried in an oven at 60°C overnight. After complete drying, the films were immersed in 5% $CaCl_2$ solution for 30 min to encourage cross-linking of the polymer chains. Lastly, the final drying was performed to acquire the complete hydrogel films.

2.4 Characterizations

The cross-section morphology of the hydrogel films was examined by a Field Emission-Scanning Electron Microscope (FE-SEM) (JSM-6000 Plus, JEOL, Japan) at 2kV with Au coating. Attenuated Total Reflectance Fourier-Transform Infrared Spectroscopy (ATR-FTIR) spectroscopy examined the chemical structures, interactions, and functional group characteristics. The spectra were measured by co-adding 32 scans at a resolution of 4 cm^{-1}. The mechanical properties of the film sheet samples were examined in tensile mode on a Tinius Olsen H5KT machine with a 1000 N load cell. The film sheet specimens were prepared at a 15 mm width. The measurements were conducted at a 50 mm gauge length at a tensile speed of 5 $mm{\cdot}min^{-1}$. Each sample was measured in 3 replicates, and the average value was reported. The water absorption rate into the nanofiber mats was investigated by cutting the fiber mat into a 3 cm^2 area. The fiber mat was weighed before and after swelling in RO water as a function of time. Each sample was measured in triplicate, and the average value was reported. Crude MPE, Polymer blends, and composites were analyzed by DSC-TGA (STD Q600) to study the thermal stability and thermal behavior.

2.5 Anti-staphylococcal activity

The disk diffusion method was used to examine antibacterial properties. Staphylococcus aureus TISTR 2329, kindly provided by the Thailand Institute of Scientific and Technology Research (TSITR), was initially cultured on Nutrient Agar (NA) medium and incubated at 37°C for 18 h. Bacterial colonies were then suspended in sterile distilled water to attain a standard turbidity of 0.5 McFarland. The bacterial suspension was uniformly spread over the surface of the NA using a sterile cotton swab. Meanwhile, the samples were cut into circular shapes with a diameter of 6 mm and a thickness of approximately 1 mm, and placed onto the prepared bacterial lawn. Sterile distilled water was used as the negative control (NTC), while penicillin at a concentration of 10 U was used as the positive control (PEN). The plates were subsequently incubated at 37°C for 24 h, after which the diameter of the clear inhibition zones was measured in millimeters using Vernier calipers from the edge boundaries of complete growth inhibition. All experiments were performed in triplicate. The average values and standard deviation were calculated, and statistical analysis was conducted using GraphPad Prism version 8.3.4, applying a paired t-test with a 95% confidence interval, with $p < 0.05$ considered statistically significant.

3. Results and discussion

3.1 Morphology

The morphological surface of the crude MPE and hydrogel films is observed in Figure 1, while the crude MPE is revealed in Figure 1(a). The ground size was about 20 µm to 40 µm, and some stuck can be increased to 200 µm to 300 µm. It is a concern that the composite films must be ground and sieved before use. The surface also shows a sharp edge with some small fibers inside. It can be from the tiny cellulose curtain passed through a synthesis method. However, other research has mentioned the advantages of fibers, which can improve the mechanical strength [19]. For the film part, neat SA in Figure 1(b) shows a smooth surface with a linear pattern, which can be seen from the clue of the wrinkling. After blending with the AV, the films provided a rough surface similar to the heterogeneous phase, as in Figure 1(c). However, the indication was well dispersed and stimuli for all areas [20]. The film can be expected to perform well, especially regarding mechanical properties. Thus, the MPE composites in Figure 1(d) show the heterogeneous agglomerated size of about 20 µm, similar to the mesh used, uniformly scattered throughout the film. The MPE fiber was covered by the SA matrix, which was well affected because it is not entirely separated from the top or sedimented to the bottom side of the films. In many composite works, the small powder in micro-nano size stayed in heterogeneous phases, still improving the mechanical strength and rigidity of the polymers [21,22].

3.2 Functional groups and chemical structures

FTIR analysis characterized the functional groups and chemical structures of the materials. The pure MPE particles are represented in the different bands at 1055 cm^{-1} and 1452 cm^{-1}, which describe the C–O stretching and CH bending in phenolic compounds and cellulose fibers. It corresponds to the FE-SEM image of the MPE particle, where some part of them looks like a short fiber feature. Additionally, the CH_3 asymmetric stretching vibration at 2950 cm^{-1} also indicates the MPE fingerprint, as shown in Figure 2(a). Figure 2(b) shows the band of SA that relates to the band at 1025 cm^{-1}, which shows the C–O stretching from the alginates' uronic acid group. Thus, the band at 1280 cm^{-1} represents the C–O stretching from the polysaccharide backbone. The COO– symmetric and asymmetric stretching were illustrated at 1410 cm^{-1} and 1590 cm^{-1}. Actually, the COO– of the alginate was observed at 1600 cm^{-1} to 1620 cm^{-1}, but in our work was shifted to 1590 cm^{-1}. It is associated with the crosslinking mechanism of the Ca^{2+} crosslink by shifting to the left-hand side at 1590 cm^{-1} after soaking in the $CaCl_2$ solution. This is entitled "Egg-Box" Model, where the primary mechanism for gelation is ionic crosslinking with divalent cations. Moreover, CH from methylene stretching is performed at 2850 cm^{-1} to and 2915 cm^{-1} for symmetric and asymmetric vibration. The free OH stretching was matched at the broad band at 3300 cm^{-1} [23-26].

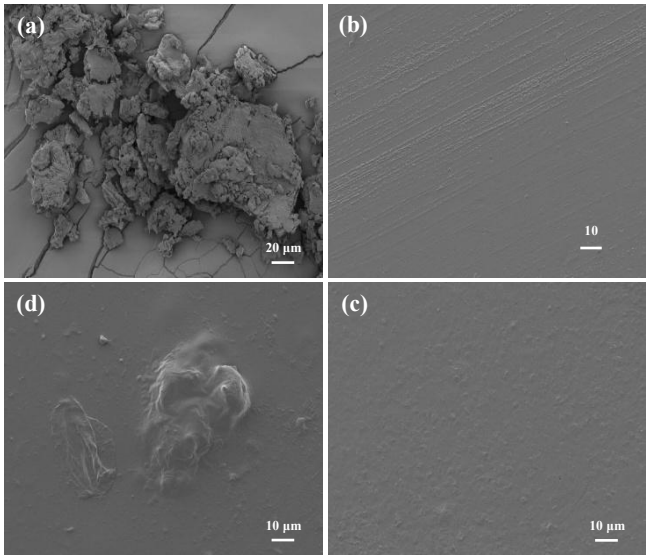

Figure 1. FE-SEM images at the surface of (a) crude MPE at 500x, (b) neat SA, (c) SA/AV, and (d) SA/AV/MPE hydrogel films at 1000x.

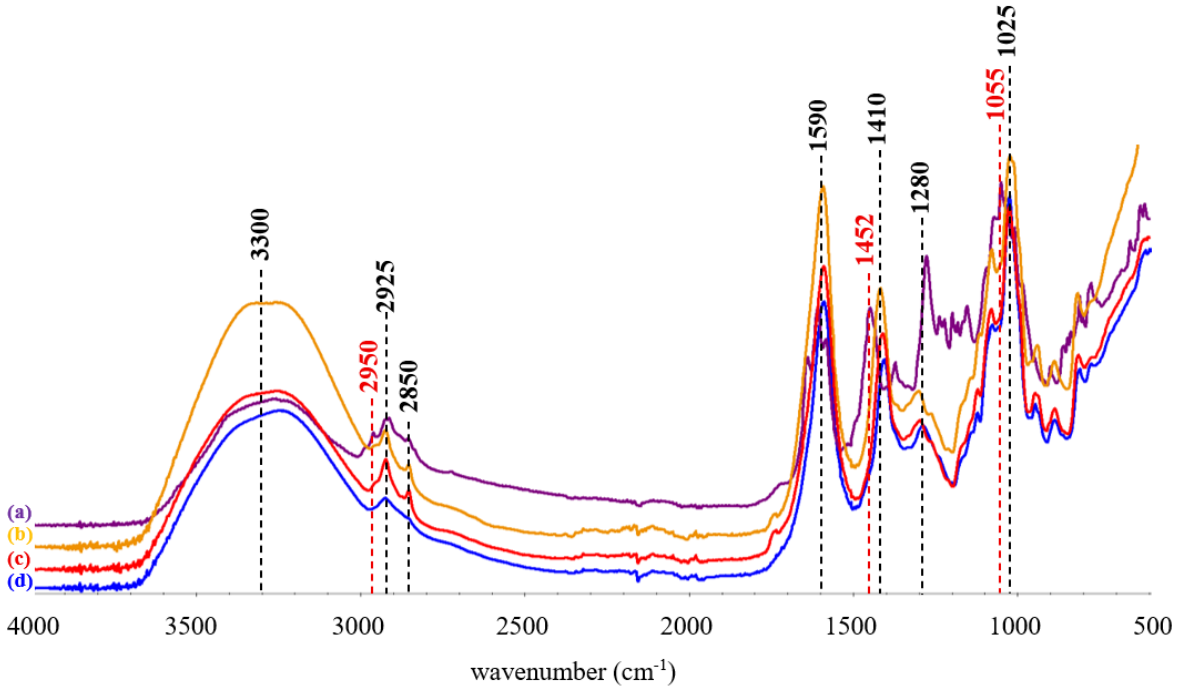

Figure 2. FTIR spectra of (a) crude MPE, (b) neat SA, (c) SA/AV, and (d) SA/AV/MPE hydrogel films.

In terms of the MPE composites also showing similar bands, because a small amount was added, which resulted in only a similar band to the matrix [27,28]. However, the significant band of MPE was affected at 2850 cm^{-1} and 2925 cm^{-1}. It can be observed that the MPE band is obscured in this case by the undetected sharp peak, while the intensity is similar [29]. It can indicate that the particle was still at the film's surface, which is commonly found by using ATR-FTIR measurement [28]. It corresponds to the FE-SEM, where the matrix polymer covers all particles inside the films. In the other parts, a slight intensity of the OH band decreasing was detected due to the lower hydrophilic chemicals such as xanthones and tannins. The area normalization found that 19% reduction, using 1590 cm^{-1} as a standard band area. Nevertheless, the aloe vera and alginate have similar functional groups of hydrocarbons and polysaccharides, which cannot distinguish between these complexation materials [8].

3.3 Mechanical properties

The mechanical properties of hydrogel films were examined using a tensile test, as shown in Figure 3. Tensile strength increases when an additive is blended with the materials, while the low mechanical strength of neat SA remains, as shown in Figure 3(a). Figure 3(b) reveals the Young's modulus with trends increasing in similarity to the tensile strength. However, it increased further when the MPE particles were added to the materials. This is because of the effects of composite materials, which provide high rigidity [27,30]. Previous works describe the cellulose and lignin particles affected similarly, increasing the strength and rigidity of polymer composites. Even though it is not the same matrix and additive, the effected of composites are provided in these trends [31,32]. Not only that, AV still acts as an elastomer for the hydrogel, because of the increasing trends that break elongation and toughness, as shown in Figure 3(c). The improvement of both strength and elongation was from the amorphous chain in AV. It helps create mobility between the chains, which perform slight movements when the film receives the force, but not too much to destroy the networks. Although the P value described the non-significant data in some of them, the error bar from the SD can be implied to a trend of change. For more support, the stress-strain curves in Figure 3(d) represent the shape of the SA/AV. It was a tougher shape, but still has some curve at the yield point, representing some crystal formation [33,34]. Thus, AV makes a balance for materials that are not too rigid for the composite of MPE, which still decreases the material's toughness but provides strong samples without cracks in the final products.

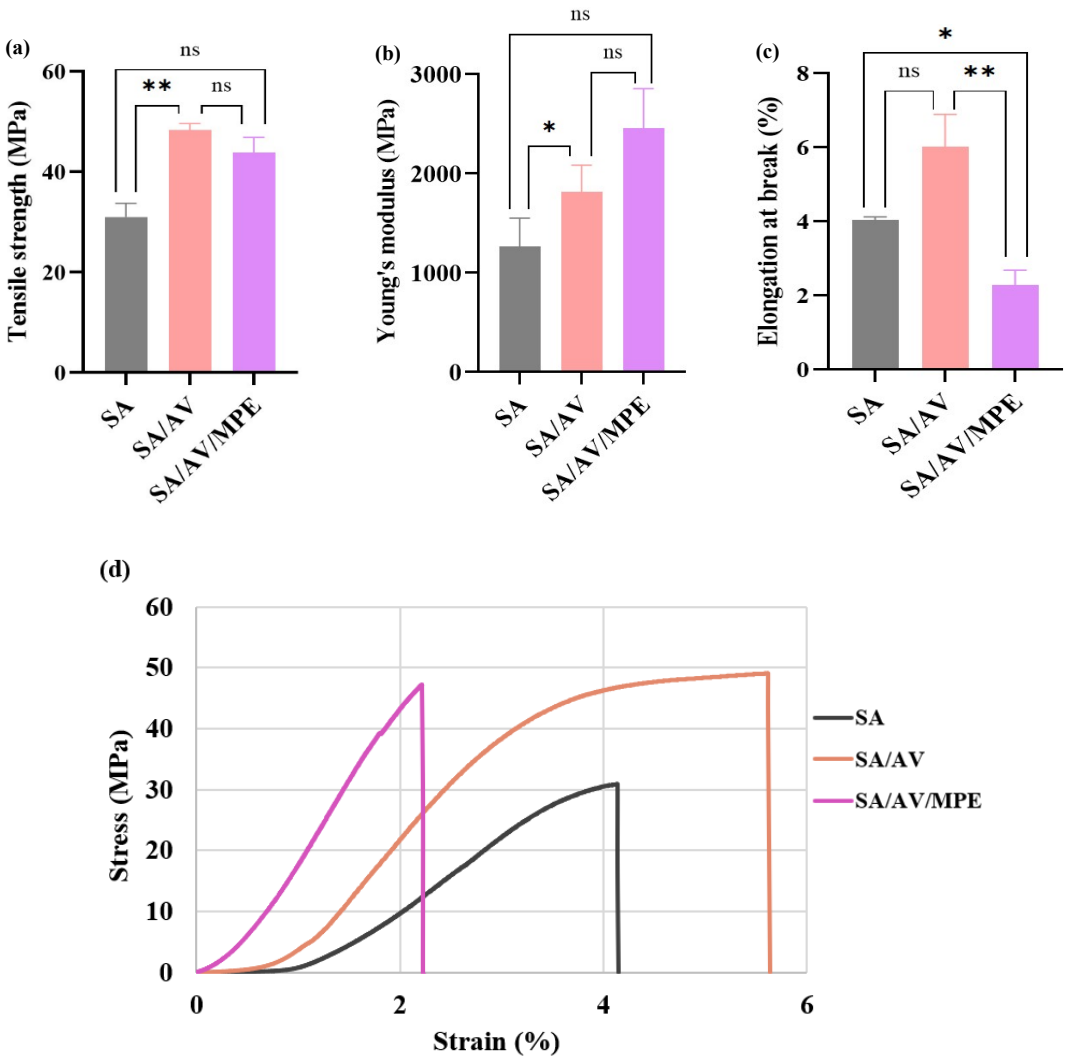

Figure 3. Mechanical properties (a) tensile strength, (b) Young's modulus, (c) elongation at break, and (d) stress-strain curves of hydrogel cast films.

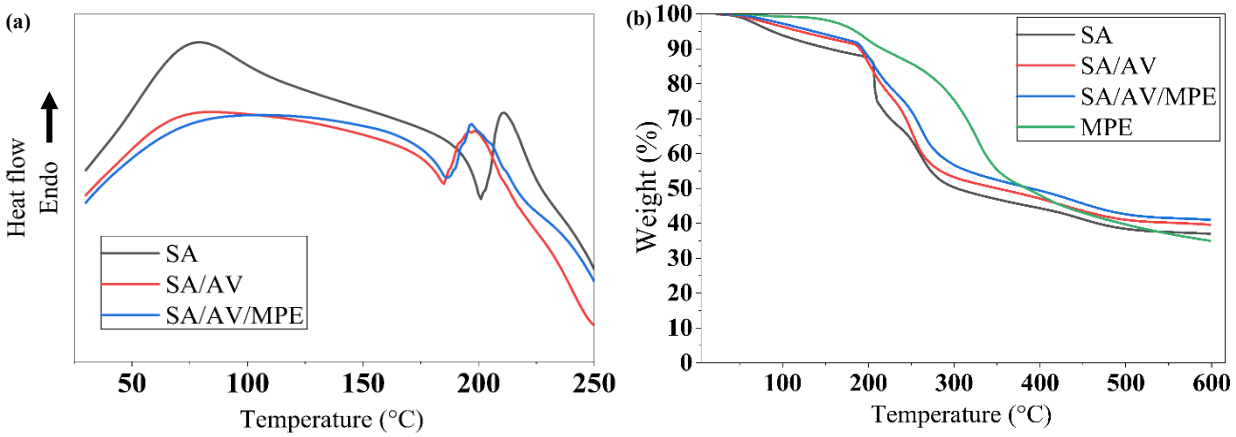

Figure 4. Thermal behavior of hydrogel by (a) DSC heat flow, and (b) TGA curves.

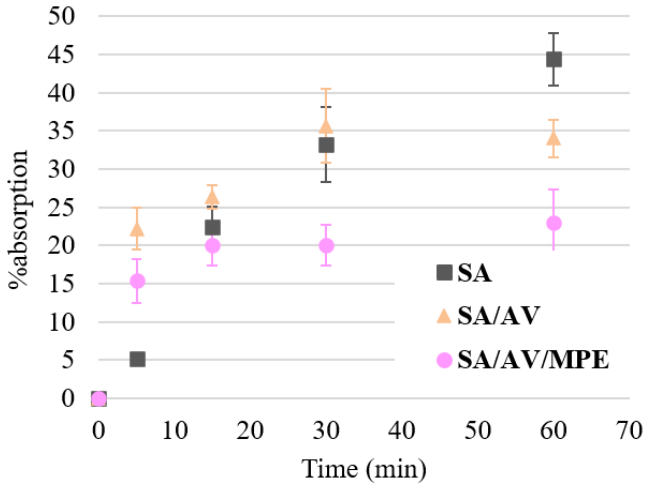

Figure 5. Water absorption capability of the hydrogel and its composites at various time points.

3.4 Thermal properties

Thermal properties of SA, SA/AV, and SA/AV/MPE hydrogels were analyzed by DSC analysis, as plotted and summarized in Figure 4(a). The phase transitions and thermal stability of neat SA, SA/AV, and SA/AV/MPE hydrogel films were evaluated by DSC-TGA analysis. From DSC curves at 65°C to 80°C, it is attributed to the dehydrated of both free and bound in the hydrophilic groups of the SA. It corresponds with the Maniania, B. Zuka, *et al.* who describe the dehydration of SA at 80°C [35]. In this position, incorporating with AV and MPE resulted in a lower shifted and reduced the intensity compared to neat SA. Describing that, a modification in the water holding capacity and dense molecular network alters the moisture necessary. At higher temperatures, neat SA exhibited the characteristic degradation starting at 204°C, representing the depolymerization of the glycosidic units. For AV blended, a secondary peak was observed about 170°C to 190°C, suggesting comparatively lower thermal resistance. It is likely because of the effected of the H-bonding from bioactive polysaccharides, such as acemannan, present in the aloe vera. It was mentioned in the same trends as Oluba, Olarewaju M., *et al.*'s work, who mentioned that this effect is attributed to the disruption of hydrogen bonding and reduced crystallinity by Aloe vera in agreement with previous research on the effects of incorporating bioactive agents in starch-based films [36].

Thermal degradation was illustrated to describe the decomposition of the hydrogels, as plotted in Figure 4(b). The results provided mainly two-step degradation without the initial decrease due to water evaporation from the moisture before 100°C. In the primary degradation region at 200°C to 220°C, SA and SA/AV demonstrated similar rapid decomposition profiles, reaching approximately 50% weight retention by 250°C to 300°C, indicating characteristic biopolymer degradation. The neat MPE shows that T_{d50} represents the higher degradation temperature. Moreover, the graphs were also confirmed by the shifted line on the right-hand side as a trend after blended AV and MPE were added. Notably, the SA/AV/MPE composite exhibited further enhancement, closely approaching the performance of neat MPE. It displayed the highest thermal resistance throughout the temperature range.

At 550°C to 600°C, all samples converged to approximately 35% to 40% residual weight, suggesting similar char formation characteristics. Even though the first step of degradation was introduced at 100°C to 200°C, which is close to with melting temperature. Some of the work describes the no T_m of SA. However, the first step was about 10% including the moisture evaporation, and the DSC can clearly observe the exothermic curves at Tm that can be illustrated. It can be described as the decreasing in the DSC thermogram baselines that befallen after the exothermic regions. These results demonstrate that MPE acts as an effective thermal stabilizer, significantly improving the high-temperature performance of SA/AV/MPE composites, which is particularly advantageous for applications requiring enhanced thermal stability [37,38].

3.5 Water absorption

Water absorption of hydrogel is a vital property for applied use in the biomedical sheet, as shown in Figure 5. The results reveal a high performance of the SA hydrogel, about 45% from dry weight at 60 min, because it completely performs a hydrogel cross-linkage [39]. After adding AV to the films, it blocked some crosslinking from its amorphous structure, which reduced the absorption ability [23]. However, almost all of AV's structures show high polarity of hydroxyl groups, so it still maintains the water inside. However, the MPE shows a significant decrease in this property. This is because the big particles of MPE obstructed

the crosslink hydrogel reaction, and the high hydrophobicity of xanthones, the main compound in MPE, decreased the water absorption [40]. Not only that, it also corresponds with the FTIR analysis, which shows the low free OH groups at 3300 cm^{-1} in MPE composite samples. It can be described that the water absorption was from the xanthones or other hydrophobic components of MPE [17]. It also corresponds with the FE-SEM, which prohibits the MPE from being covered inside the films.

Lei H. and Peiyi W. describe the H-bonding and bridge structure of SA using 2D-FTIR and ATR-FTIR to confirm that the H–bonding is reduced when the temperature changing. They define the inter/intramolecular hydrogen bonding within SA chains, such as $O_3H_3\cdots O_5$ and $O_2H_2\cdots O{=}C{-}O{-}$. All of the bonds lead to the appearance of relatively free –OH and COO– groups. Corresponding with our FTIR results, which observed the lower OH with lower water absorption in the same trends [41]. The particles provided the roughness surface, which affected the hydrophobicity. Sachdev D. *et al.* mentioned that the effected of hydrophobicity and water absorption are the material degradation, environment conditions, chemical composition, heterogeneity, porous, and surface morphology [42]. The surface was affected by water absorption when there was too high a water contact angle. In this case, slight roughness exhibits a slower rate of absorption, as the %absorption was affected by other reasons. By the way, in our work, the degradation and environment were not mentioned as being out of scope; the others were evaluated. Although reducing the composites' hydrogel was found, it still has a capability of about 20% of the dry weight. On the other hand, previous works described that more hydrophobic materials also provide better antibacterial properties, which is related to a beneficial way for this work [43-45].

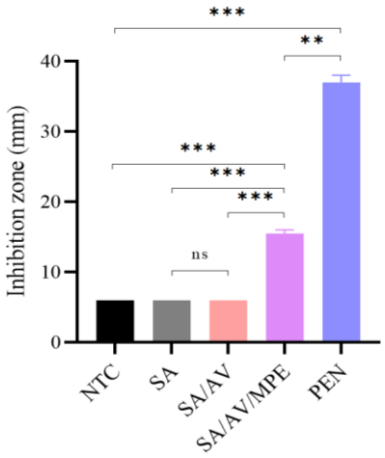

Figure 6. Anti-staphylococcal activity of SA, SA/AV, and SA/AV/MPE hydrogel films determined by the disk diffusion method. Data is presented as mean ± SD of inhibition zone diameters in mm. (ns, not significant; ** $p \leq 0.01$, *** $p \leq 0.001$, paired t test, 95% confidence interval).

Table 1. Clear inhibition zone of hydrogel films against *Staphylococcus aureus*.

Sample	Inhibition zone [mm]
NCT	6 ± 0
SA	6 ± 0
SA/AV	6 ± 0
SA/AV/MPE	15 ± 1
PEN	37 ± 1

3.6 Anti-staphylococcal property

According to data from the World Health Organization (WHO), millions of patients suffer from bacterial infections per year [46]. *Staphylococcus aureus* is the most lethal bacteria associated with wound infections, antibiotic resistance, and numerous severe complications [47-49]. Therefore, antibacterial activity is an essential property that should be considered for any materials with potential applications in wound dressing and biomedical settings. The antimicrobial activity against *Staphylococcus aureus* of three distinct fabricated hydrogel films, namely, SA, SA/AV, and SA/AV/MPE, was evaluated using the disk diffusion method [50]. The results revealed that the SA/AV/MPE hydrogel film exhibited noticeable antibacterial activity, as evidenced by a clear inhibition zone measuring 15 ± 1 mm. In comparison, the SA and SA/AV hydrogel films exhibited unobservable inhibitory effects on bacterial growth, as indicated by the bacterial growth extending to the edge of the 6 mm disk, as shown in

Statistical analysis demonstrated that, although the inhibition zone of SA/AV/MPE was smaller than that of the penicillin control ($p \leq 0.01$), it was significantly greater than those of both SA and SA/AV hydrogel films ($p \leq 0.001$). The absence of a statistically significant difference between the SA and SA/AV formulations indicated that the incorporation of aloe vera alone did not confer measurable anti-staphylococcal activity. In contrast, the marked increase in the inhibition zone observed following the addition of MPE highlights its critical role in enhancing the anti-staphylococcal performance of the composite hydrogel, as shown in Figure 6. The observed antibacterial effect is attributable to the presence of bioactive compounds constituents in MPE, such as xanthones, tannins, and phenolic acids, which have been previously reported with antimicrobial properties [51-53]. Summarily, these results illuminated the potential of SA/AV/MPE hydrogel film as a functional material for applications in wound dressing and other biomedical settings.

4. Conclusions

The SA hydrogels and their blends showed that the 10% w/v can be processed via a cast film process. A morphological analysis of the films exhibited excellent dispersion between SA and AV but resulted in a heterogeneous structure when the MPE was composited. FTIR analysis indicated almost the same band between SA and AV, but a slight difference in MPE-cooperated films. It also promoted that the lower polar functional groups of OH in FTIR resulted in a lower water absorption of hydrogel blends and composites. However, the deeply investigate into crosslinking details is available for future work. This point can promote better dispersion, while the easy processable should be maintained. The mechanical analysis showed that the SA/AV film exhibited improved mechanical properties, but the elongation decreased when the MPE was incorporated. Thermal properties revealed that the AV and MPE led to decreases in T_g and T_m, as all of the hydrogels showed non-crystalline polymer characteristics. However, the thermal degradation was improved when AV and MPE were additionally composed. In addition, the antibacterial testing demonstrated a favorable enhancement when MPE was introduced into the SA/AV hydrogel film sheet. Summarily, the results indicated that the SA/AV/MPE composite film represents a promising alternative

material for applications in bandages, wound dressings, and other biomedical materials.

Acknowledgments

This research is supported by the Student Quality Development (SQD) and Parent-Teacher Association (PTA) budgets of The Demonstration School of Bansomdejchaopraya Rajabhat University. Special appreciation to Asst. Prof. Dr. Jariwat Siriin from the Department of Biology, Faculty of Education, Bansomdejchaopraya Rajabhat University. For characterizations, sincerely thanks to the Center of Excellence in Functional Advanced Materials Engineering (CoE FAME), Sirindhorn International Institute of Technology (SIIT), Thammasat University. Additionally, Prof. Dr. Piyasan Praserthdam, who is a member of the Center of Excellence on Catalysis and Catalytic Reaction Engineering, Department of Chemical Engineering, Faculty of Engineering, Chulalongkorn University. Lastly, Assoc. Prof. Dr. Sirirat Wacharawichanant, from the Polymer Innovation (PI) Laboratory, Department of Chemical Engineering, Faculty of Engineering and Industrial Technology, Silpakorn University.

References

[1] S. Buaruk, P. Somnuake, S. Gulyanon, S. Deepaisarn, S. Laitrakun, and P. Opaprakasit, "Membrane filter removal in FTIR spectra through dictionary learning for exploring explainable environmental microplastic analysis," *Scientific Reports,* vol. 14, no. 1, p. 20297, 2024.

[2] A. S. Thar, S. Laitrakun, P. Somnuake, S. Deepaisarn, P. Opaprakasit, K. Athikulwongse, M. Yamaguch, and S. Gulyanon, "Enhancing microplastic classification through filter-interfered FTIR spectra using dimensionality reduction and deep learning in low-dimensional spaces," *Marine Pollution Bulletin,* vol. 221, p. 118548, 2025.

[3] K. I. Draget, G. Skjåk-Bræk, and O. Smidsrød, "Alginate based new materials," *International journal of biological macromolecules,* vol. 21, no. 1–2, pp. 47–55, 1997.

[4] H. Hecht, and S. Srebnik, "Structural characterization of sodium alginate and calcium alginate," *Biomacromolecules,* vol. 17, no. 6, pp. 2160-2167, 2016.

[5] N. K. Sachan, S. Pushkar, A. Jha, and A. Bhattcharya, "Sodium alginate: The wonder polymer for controlled drug delivery," *Journal of Pharmacy Research,* vol. 2, no. 8, pp. 1191–1199, 2009.

[6] B. Roopa, and S. Bhattacharya, "Alginate gels: I. Characterization of textural attributes," *Journal of Food Engineering,* vol. 85, no. 1, pp. 123–131, 2008.

[7] H. Wang, L. Yang, and Y. Yang, "A review of sodium alginate-based hydrogels: Structure, mechanisms, applications, and perspectives," *International Journal of Biological Macromolecules,* vol. 292, p. 139151, 2025.

[8] R. Pereira, A. Mendes, and P. Bártolo, "Alginate/Aloe vera hydrogel films for biomedical applications," *Procedia CIRP,* vol. 5, pp. 210–215, 2013.

[9] B. Ishfaq, I. U. Khan, S. H. Khalid, and S. Asghar, "Design and evaluation of sodium alginate-based hydrogel dressings containing Betula utilis extract for cutaneous wound healing," *Frontiers in Bioengineering and Biotechnology,* vol. 11, p. 1042077, 2023.

[10] R. Pereira, A. Carvalho, D. C. Vaz, M. Gil, A. Mendes, and P. Bártolo, "Development of novel alginate based hydrogel films for wound healing applications," *International journal of biological macromolecules,* vol. 52, pp. 221–230, 2013.

[11] M. Chelu, A. M. Musuc, M. Popa, and J. Calderon Moreno, "Aloe vera-based hydrogels for wound healing: Properties and therapeutic effects," *Gels,* vol. 9, no. 7, p. 539, 2023.

[12] Y. S. Lim, S. S. H. Lee, and B. C. Tan, "Antioxidant capacity and antibacterial activity of differentparts of mangosteen (Garcinia mangostana Linn.) extracts," *Fruits,* vol. 68, no. 6, pp. 483–489, 2013.

[13] W. Suttirak, and S. Manurakchinakorn, "In vitro antioxidant properties of mangosteen peel extract," *Journal of food science and technology,* vol. 51, no. 12, pp. 3546–3558, 2014.

[14] T. Shan, Q. Ma, K. Guo, J. Liu, W. Li, F. Wang, and E. Wu, "Xanthones from mangosteen extracts as natural chemopreventive agents: Potential anticancer drugs," *Current molecular medicine,* vol. 11, no. 8, pp. 666–677, 2011.

[15] H. T. Nguyen, T. T. Nguyen, H. T. Do, L. V. K. Bui, T. A. Nguyen, H. T. Nguyen, and T. T. Thi, "Hydrogel based on cellulose and mangosteen rind extract with antibacterial activity: Preparation and characterization," *Biopolymers,* vol. 116, no. 3, p. e70024, 2025.

[16] N. Kusumawati, A. B. Santoso, M. M. Sianita, and S. Muslim, "Extraction, characterization, and application of natural dyes from the fresh mangosteen (Garcinia mangostana L.) peel," *International Journal on Advanced Science, Engineering and Information Technology,* vol. 7, no. 3, pp. 878–884, 2017.

[17] W. Widowati, L. Darsono, J. Suherman, Y. Yelliantty, and M. Maesaroh, "High performance liquid chromatography (HPLC) analysis, antioxidant, antiaggregation of mangosteen peel extract (Garcinia mangostana L.)," *International Journal of Bioscience, Biochemistry and Bioinformatics,* vol. 4, no. 6, pp. 458–466, 2014.

[18] B. Ovalle-Magallanes, D. Eugenio-Pérez, and J. Pedraza-Chaverri, "Medicinal properties of mangosteen (Garcinia mangostana L.): A comprehensive update," *Food and Chemical Toxicology,* vol. 109, pp. 102–122, 2017.

[19] L. Zhou, K. Ke, M.-B. Yang, and W. Yang, "Recent progress on chemical modification of cellulose for high mechanical-performance Poly (lactic acid)/Cellulose composite: A review," *Composites Communications,* vol. 23, p. 100548, 2021.

[20] J. Y. Chung, A. J. Nolte, and C. M. Stafford, "Surface wrinkling: A versatile platform for measuring thin-film properties," *Advanced materials,* vol. 23, no. 3, pp. 349–368, 2011.

[21] B. E. Arteaga-Ballesteros, A. Guevara-Morales, E. S. Martín-Martínez, U. Figueroa-López, and H. Vieyra, "Composite of polylactic acid and microcellulose from kombucha membranes," *e-Polymers,* vol. 21, no. 1, pp. 015–026, 2020.

[22] J. Cao, Y. Gao, G. Li, B. He, S. Ren, Y. Bai, and F. Wang, "A facile method for carbon nanotube/carbon fiber-reinforced polylactic acid composites," *Polymer Composites,* vol. 46, no. 3, pp. 2772–2780, 2024.

[23] R. Pereira, A. Tojeira, D. C. Vaz, A. Mendes, and P. Bártolo, "Preparation and characterization of films based on alginate and aloe vera," *International Journal of Polymer Analysis and Characterization,* vol. 16, no. 7, pp. 449–464, 2011.

[24] C. Badita, D. Aranghel, C. Burducea, and P. Mereuta, "Characterization of sodium alginate based films," *Romanian Journal of Physics,* vol. 65, no. 1–2, pp. 1–8, 2020.

[25] Z. Belattmania, S. Kaidi, E. A. Samir, C. Katif, F. Bentiss, C. Jama, A. Reani, B. Sabour, and V. Vasconcelos, "Isolation and FTIR-ATR and 1H NMR characterization of alginates from the main alginophyte species of the atlantic coast of Morocco," *Molecules,* vol. 25, no. 18, p. 4335, 2020.

[26] M. Z. Mollah, M. R. Faruque, D. Bradley, M. U. Khandaker, and S. Al Assaf, "FTIR and rheology study of alginate samples: Effect of radiation," *Radiation Physics and Chemistry,* vol. 202, p. 110500, 2023.

[27] S. Wacharawichanant, N. Wimonsupakit, and S. Kuhaudomlap, "Comparison of morphology and mechanical properties of polyoxymethylene/cellulose and poly(lactic acid)/cellulose composites," *Materials Science Forum,* vol. 916, pp. 19–23, 2018.

[28] J. Grdadolnik, "ATR-FTIR spectroscopy: Its advantage and limitations," *Acta Chimica Slovenica,* vol. 49, no. 3, pp. 631–642, 2002.

[29] N. Wathoni, N. Yuniarsih, A. Cahyanto, and M. Muhctaridi, "α-Mangostin hydrogel film based chitosan–alginate for recurrent aphthous stomatitis," *Applied Sciences,* vol. 9, no. 23, p. 5235, 2019.

[30] S. Van Nguyen, and B. K. Lee, "Polyvinyl alcohol/cellulose nanocrystals/alkyl ketene dimer nanocomposite as a novel biodegradable food packing material," *International Journal of Biological Macromolecules,* vol. 207, pp. 31–39, 2022.

[31] W. Teeka, K. Srisujaritpanich, P. Somnuake, and S. Wacharawichanant, "Development of biodegradable poly (lactic acid)/lignin treated alkyl ketene dimer properties for packaging applications," *Advances in Science and Technology,* vol. 150, pp. 11–20, 2024.

[32] P. Somnuake, P. Puttawong, and S. Wacharawichanant, "Morphology and properties of poly (lactic acid)/ethylene propylene diene monomer blends with micro-cellulose fibers from paper pulp," *Advances in Science and Technology,* vol. 150, pp. 3–10, 2024.

[33] Y. V. Milman, I. Gridneva, and A. Golubenko, "Construction of stess-strain curves for brittle materials by indentation in a wide temperature range," *Science of Sintering,* vol. 39, no. 1, pp. 67–75, 2007.

[34] M. A. AlMaadeed, S. Labidi, I. Krupa, and M. Ouederni, "Effect of waste wax and chain structure on the mechanical and physical properties of polyethylene," *Arabian Journal of Chemistry,* vol. 8, no. 3, pp. 388–399, 2015.

[35] B. Z. Maniania, M. M. Senzedi, J. M. Tsumbu, A. M. Bafubiandi, R. B. M. Lepiba, and L. Eyumu, "Study of the adsorption of nickel ions on sodium alginate polymeric membrane in hydro-metallurgical effluents: étude de l'adsorption des ions de nickel sur une membrane polymérique d'alginate de sodium dans les effluents hydrométallurgiques," *Revue Congolaise des Sciences et Technologies,* vol. 3, no. 1, pp. 121–129, 2024.

[36] O. M. Oluba, S. Muthusamy, N. Subbiah, and T. Palanisamy, "Sustainable packaging using Aloe vera infused mango starch–wool keratin biocomposite films to extend the shelf life of mango," *Scientific Reports,* vol. 15, no. 1, p. 29098, 2025.

[37] T. M. Swamy, B. Ramaraj, and Siddaramaiah, "Sodium alginate and poly (ethylene glycol) blends: Thermal and morphological behaviors," *Journal of Macromolecular Science, Part A: Pure and Applied Chemistry,* vol. 47, no. 9, pp. 877–881, 2010.

[38] S. B. Shah, C. P. Patel, and H. C. Trivedi, "Thermal behaviour of graft copolymers of sodium alginate," *Die Angewandte Makromolekulare Chemie: Applied Macromolecular Chemistry and Physics,* vol. 235, no. 1, pp. 1–13, 1996.

[39] A. El Idrissi, O. Dardari, F. N. N. N. Metomo, Y. Essamlali, A. Akil, O. Amadine, S. Adoulhrouz, and M. Zahouily, "Effect of sodium alginate-based superabsorbent hydrogel on tomato growth under different water deficit conditions," *International Journal of Biological Macromolecules,* vol. 253, p. 127229, 2023.

[40] N. A. Mohammad, D. N. A. Zaidel, I. I. Muhamad, M. A. Hamid, H. Yaakob, and Y. M. M. Jusoh, "Optimization of the antioxidant-rich xanthone extract from mangosteen (Garcinia mangostana L.) pericarp via microwave-assisted extraction," *Heliyon,* vol. 5, no. 10, 2019.

[41] L. Hou, and P. Wu, "Exploring the hydrogen-bond structures in sodium alginate through two-dimensional correlation infrared spectroscopy," *Carbohydrate polymers,* vol. 205, pp. 420–426, 2019.

[42] D. Sachdev, S. Gupta, N. K. Bhullar, and G. Verma, "Recent progress on the correlation between hydrophobicity and the water absorption of different materials," *Journal of Inorganic and Organometallic Polymers and Materials,* pp. 1–26, 2025.

[43] K. Bartlet, S. Movafaghi, L. P. Dasi, A. K. Kota, and K. C. Popat, "Antibacterial activity on superhydrophobic titania nanotube arrays," *Colloids and Surfaces B: Biointerfaces,* vol. 166, pp. 179–186, 2018.

[44] P. Somnuake, P. Opaprakasit, and A. Petchsuk, "Electrospun nanofibers of polylactide (PLA) stereocomplex with super-hydrophobic surfaces for potential use in facial mask and bio-medical applications," Thammasat University, 2021.

[45] U. Eduok, J. Szpunar, and E. Ebenso, "Superhydrophobic anti-bacterial polymer coatings," in *Superhydrophobic Polymer Coatings*, 2019, pp. 245–279.

[46] Z. Cao, Y. Luo, Z. Li, L. Tan, X. Liu, C. Li, Y. Zheng, Z. Cui, K. Yeung, Y. Liang, S. Zhu, and S. Wu, "Antibacterial hybrid hydrogels," (in eng), *Macromolecular Bioscience,* vol. 21, no. 1, p. e2000252, 2021.

[47] GBD 2019 Antimicrobial Resistance Collaborators, "Global mortality associated with 33 bacterial pathogens in 2019: A systematic analysis for the Global Burden of Disease Study 2019," *The Lancet,* vol. 400, no. 10369, pp. 2221–2248, 2022.

[48] A. H. Rasmi, E. F. Ahmed, A. M. A. Darwish, and G. F. M. Gad, "Virulence genes distributed among Staphylococcus aureus causing wound infections and their correlation to antibiotic resistance," (in eng), *BMC Infectious Diseases,* vol. 22, no. 1, p. 652, 2022.

[49] Y. Guo, G. Song, M. Sun, J. Wang, and Y. Wang, "Prevalence and Therapies of Antibiotic-Resistance in Staphylococcus aureus," (in eng), *Frontiers in Cellular and Infection Microbiology,* vol. 10, p. 107, 2020.

[50] D. M. Rata, A. N. Cadinoiu, M. Popa, L. I. Atanase, O. M. Daraba, I. Popescu, L. E. Romila, and D. L. Ichim, "Biocomposite hydrogels for the treatment of bacterial infections: Physico-chemical characterization and in vitro assessment," (in eng), *Pharmaceutics,* vol. 13, no. 12, p. 2079, 2021.

[51] S. Narasimhan, S. Maheshwaran, I. A. Abu-Yousef, A. F. Majdalawieh, J. Rethavathi, P. E. Das, and P. Poltronieri, "Anti-bacterial and anti-fungal activity of xanthones obtained via semi-synthetic modification of α-mangostin from garcinia mangostana," (in eng), *Molecules,* vol. 22, no. 2, p. 275, 2017.

[52] W. Pothitirat, M. T. Chomnawang, R. Supabphol, and W. Gritsanapan, "Comparison of bioactive compounds content, free radical scavenging and anti-acne inducing bacteria activities of extracts from the mangosteen fruit rind at two stages of maturity," (in eng), *Fitoterapia,* vol. 80, no. 7, pp. 442–447, 2009.

[53] K. Phumlek, A. Itharat, P. Pongcharoen, P. Chakkavittumrong, H-Y. Lee, G-S. Moon, M-H. Han, S. Panthong, W. Ketjinda, and N. M. Davies, "Garcinia mangostana hydrogel patch: bactericidal activity and clinical safety for acne vulgaris treatment," (in eng), *Research in Pharmaceutical Sciences,* vol. 17, no. 5, pp. 457–467, 2022.